ELSEVIER

Engineering Analysis with Boundary Elements 31 (2007) 812–818

ENGINEERING ANALYSIS with BOUNDARY ELEMENTS

www.elsevier.com/locate/enganabound

A mixed surface integral formulation for frequency-dependent inductance calculation of 3D interconnects

Wenjian Yu*, Changhao Yan, Zeyi Wang

Department of Computer Science & Technology, Tsinghua University, Beijing 100084, China

Received 7 November 2006; accepted 20 March 2007
Available online 24 May 2007

Abstract

A surface integral formulation based on direct boundary integral equation (BIE) was recently proposed for inductance or impedance calculation of 3D electric structures. Though faster than other volume integral methods, this formulation still suffers from as many as $7N$ unknowns, where N is the number of panels. A mixed surface integral formulation is proposed in this paper, which combines indirect BIE of double-layer potentials within conductor and the direct BIE within dielectric. With this mixed formulation, the number of unknowns is cut down from $7N$ to $4N$, and correspondingly, the CPU time for solving the linear equation system is reduced remarkably. Two interconnect structures are simulated to validate the proposed method.

Keywords: Boundary integral equation; Double-layer potential; Helmholtz equation; Inductance calculation; Surface discretization; Electro-magnetic simulation

1. Introduction

Fast 3D electro-magnetic simulation is increasingly important in the area of on-chip interconnect analysis, packaging, and microwave/RF engineering [1]. The inductive effect plays a more and more crucial role in circuit simulation and layout verification with the increasing frequency. Consequently, it is urgent to find accurate and efficient methods for calculating (extracting) the frequency-dependent inductance of 3D interconnects.

The partial element equivalent circuit (PEEC) method, a volume element method, introduced in [2] has gained the most popularity for its wide applicability. However, this method has to empoly very fine discretization to handle high frequency problems because the current distribution becomes severely uneven within conductor. Besides, for bulky conductors such as substrates, volume discetization leads to a large number of elements. Under these circumstances, such volume element method becomes very costly. Although an entire-domain basis scheme was proposed in [3] to remedy the situation, it seems difficult for this method to lead to a fast Maxwell's equation solver [4].

Recently, another approach to address this issue was proposed for 3D impedance (including inductance and resistance) extraction, based on a surface integral formulation [5]. It overcomes the shortcomings of the volume based methods and is suitable for wide-band simulations under MQS (magneto-quasistatic), EMQS (electro-magneto-quasistatic) and even full-wave assumption. Further numerical improvements were then proposed for this boundary integral formulation [4,6]. However, its main disadvantage is the large number of unknowns which is up to $6N + U$ for MQS simulation, where N and U are the numbers of panels and vertexes, respectively.

The surface integral formulation in [5] is actually a direct boundary element method (BEM), employing the direct boundary integral equation (BIE). Different from this formulation, a method of impedance extraction based on indirect BIE was proposed in [7], whose key advantage is only involving the smallest number of unknowns ($3N$). The inside idea is the minimum-order

*Corresponding author. Tel.: +86 10 62773440; fax: +86 10 62781489.
E-mail addresses: yu-wj@tsinghua.edu.cn (W. Yu), yanch@fudan.edu.cn (C. Yan), wangzy@tsinghua.edu.cn (Z. Wang).

0955-7997/$ - see front matter © 2007 Elsevier Ltd. All rights reserved.
doi:10.1016/j.enganabound.2007.03.004

BIE for 3D eddy current problem, introduced in Mayergoyz's classic paper [8] and further improved by Yuan and Kost [9]. However, this indirect BIE based method can only handle straight conductors well. This severe constraint on geometry makes it unsuitable for practical 3D interconnect extraction.

A mixed surface integral formulation for extracting frequency-dependent inductance of 3D interconnects is presented in this paper. In this method, the electric field $\vec{E}$ within conductors is expressed as double-layer potentials produced by imaginary dipole distribution on conductor surface. This is a kind of indirect BIE. While for the domain within dielectric, or among the conductors, the direct BIEs are established. Combining both kinds of BIEs, a mixed surface integral formulation is formed. The main merit of this method is that the number of unknowns can be cut down from about $7N$ to $4N$ for MQS simulation, and the CPU time can be saved by solving a smaller linear equation system. In fact, the mixed method is equivalent to the method in [5] except replacing the direct BIE within conductor by indirect BIE. Hence, the proposed method can also handle complex geometry and adapt to wide-band simulation.

The rest of this paper is organized as follows. Section 2 outlines the direct boundary integral formulation proposed in [5]. In Section 3, the mixed boundary integral formulation is presented. The numerical results with 3D interconnect structures are given in Section 4, demonstrating the advantage of the proposed method. Finally, conclusions are drawn in Section 5.

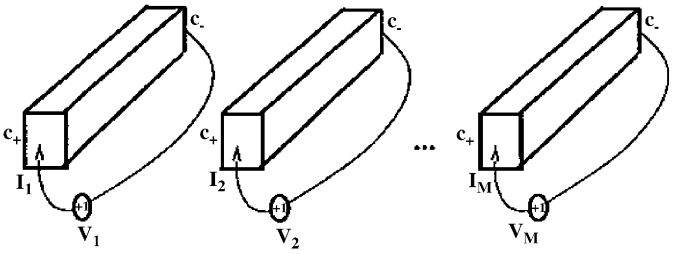

Fig. 1. Multiple conductor structure for inductance extraction.

2. Direct BIEs

Fig. 1 shows a structure including M interconnect conductors. The sinusoidal voltage V at frequency f is set between two ends, i.e. the contact surfaces c_+ and c_- in Fig. 1, where the "+" and "−" indicate the polarity of voltage. Usually, the voltage drop of one conductor (main conductor) is 1 V and the others' are 0 V. Then, the problem of inductance extraction is converted to compute the current in each conductor by solving the Maxwell's equations.

If all currents of conductors are obtained, we can represent them as a column vector I_1. Changing the main conductor setting and recomputing corresponding currents of conductors, one can obtain the other current vectors $I_2, \ldots, I_M$. Finally, with the current matrix $I = [I_1, I_2, \ldots, I_M]$, we have $ZI = \mathbf{1}$, where $\mathbf{1}$ is the identity matrix. So,

$$Z = I^{-1} \quad \text{and} \quad R = real(Z), \quad L = imag(Z)/\mathrm{i}\omega,$$

where Z, R and L are the impedance, resistance and inductance matrix, respectively, and $\omega = 2\pi f$ is the angular frequency. The key problem of inductance extraction is how to compute the currents in conductors when voltage drops are given.

Ref. [5] proposed a set of surface integral formulations for 3D impedance extraction which is suitable for MQS, EMQS and even full-wave extraction. For simplicity, we only discuss the MQS simulation in this paper and list the differential equations (left) and corresponding BIEs or boundary conditions (right) in Table 1, where $\vec{E}$ is electric field vector, φ is electric potential, $\vec{J}$ is current density, and $\vec{A}$ is magnetic vector potential. $\vec{E}_t$ and E_n denote the tangential and normal components of $\vec{E}$, respectively. μ and σ are the permeability and conductivity, respectively, and both are constants.

The vector Helmholtz equation in Table 1:

$$\nabla^2 \vec{E} - \mathrm{i}\omega\mu\sigma \vec{E} = 0 \tag{1}$$

is the most important. This vector equation can be decomposed into three scalar-valued Helmholtz equations

Table 1
Differential and boundary integral formulae for 3D impedance extraction [5]

	Governing differential equations	Boundary integral equations
For domain in each conductor	$\nabla^2 \vec{E} - \mathrm{i}\omega\mu\sigma \vec{E} = 0$	$\to \int G_1(\mathbf{y},\mathbf{x}) \frac{\partial \vec{E}(\mathbf{x})}{\partial n_x} \mathrm{d}\mathbf{x} - \int \frac{\partial G_1(\mathbf{y},\mathbf{x})}{\partial n_x} \vec{E}(\mathbf{x}) \mathrm{d}\mathbf{x} = \frac{1}{2}\vec{E}(\mathbf{y})$
	$\nabla \cdot \vec{E} = 0$	$\to \int_c \vec{E}_t(\mathbf{y}) \cdot (\vec{n}(\mathbf{y}) \times \vec{l}(\mathbf{y})) \mathrm{d}\mathbf{y} - \int_a \frac{\partial E_n(\mathbf{x})}{\partial n_x} \mathrm{d}\mathbf{x} = 0$
For domain among conductors	$\nabla^2 \vec{E} = \mathrm{i}\omega\mu \vec{J}$ $-\nabla\varphi = \vec{E} + \mathrm{i}\omega \vec{A}$ $\vec{A} = \int \mu G_0(\mathbf{y},\mathbf{x}) \vec{J}(\mathbf{x}) \mathrm{d}\mathbf{x}$	$\to \int_s G_0(\mathbf{y},\mathbf{x}) \frac{\partial \vec{E}(\mathbf{x})}{\partial n_x} \mathrm{d}\mathbf{x} - \int_s \frac{\partial G_0(\mathbf{y},\mathbf{x})}{\partial n_x} \vec{E}(\mathbf{x}) \mathrm{d}\mathbf{x} + \nabla\varphi(\mathbf{y}) = 0$
On non-contact surface		$E_n(\mathbf{y}) = 0$
On contact surface		$\varphi(\mathbf{y}) = constant$ $\frac{\partial E_n(\mathbf{y})}{\partial n_y} = 0$

under the Cartesian coordinate system:

$$\nabla^2 E_\alpha - \mathrm{i}\omega\mu\sigma E_\alpha = 0, \quad \alpha = x, y, z. \tag{2}$$

Then, each scalar-valued Helmholtz equation can be transformed into a direct BIE like

$$\int G_1(\mathbf{y},\mathbf{x})\frac{\partial E_\alpha(\mathbf{x})}{\partial n_x}\,\mathrm{d}\mathbf{x} - \int \frac{\partial G_1(\mathbf{y},\mathbf{x})}{\partial n_x} E_\alpha(\mathbf{x})\,\mathrm{d}\mathbf{x} = \frac{1}{2}E_\alpha(\mathbf{y}), \tag{3}$$

where $G_1(\mathbf{y},\mathbf{x}) = \mathrm{e}^{-\mathrm{i}kr(\mathbf{y},\mathbf{x})}/4\pi r(\mathbf{y},\mathbf{x}), k = \sqrt{-\mathrm{i}\omega\mu\sigma}$, $\mathbf{y}$ is evaluation point, $\mathbf{x}$ is field point for integration, and $r(\mathbf{y},\mathbf{x})$ is the distance between the two points. The integrals are taken on the surface of each conductor.

Combining the three scalar-valued BIEs, we obtain a single equation involving vector terms:

$$\int G_1(\mathbf{y},\mathbf{x})\frac{\partial \vec{E}(\mathbf{x})}{\partial n_x}\,\mathrm{d}\mathbf{x} - \int \frac{\partial G_1(\mathbf{y},\mathbf{x})}{\partial n_x}\vec{E}(\mathbf{x})\,\mathrm{d}\mathbf{x} = \frac{1}{2}\vec{E}(\mathbf{y}), \tag{4}$$

which is also shown in Table 1.

In Table 1, the differential equations

$$\begin{cases} \nabla^2\vec{E} = \mathrm{i}\omega\mu\vec{J}, \\ -\nabla\varphi = \vec{E} + \mathrm{i}\omega\vec{A}, \\ \vec{A} = \int \mu G_0(\mathbf{y},\mathbf{x})\vec{J}(\mathbf{x})\,\mathrm{d}\mathbf{x} \end{cases} \tag{5}$$

and the corresponding integral equation

$$\int_s G_0(\mathbf{y},\mathbf{x})\frac{\partial \vec{E}(\mathbf{x})}{\partial n_x}\,\mathrm{d}\mathbf{x} - \int_s \frac{\partial G_0(\mathbf{y},\mathbf{x})}{\partial n_x}\vec{E}(\mathbf{x})\,\mathrm{d}\mathbf{x} + \nabla\varphi(\mathbf{y}) = 0, \tag{6}$$

are also important. They are decomposed into two tangential directions under the local coordinate system. The integrands of G_0 and $\partial G_0/\partial n$ are the fundamental solution of the Laplace equation and its normal derivative, respectively.

Note that (1) and (4) depict the electro-magnetic effects among the panels within the same conductor. However, (5) and (6) are the equations for medium domain and they depict the effects among all panels from different conductors. This difference results in the fact that, the proximity effect at high frequency is caused by (5) and (6). Therefore, (5) and (6) should be kept for any kind of boundary integral formulation, if considering the proximity effect.

To solve the integral equations and boundary conditions in Table 1, the conductor surfaces are discretized into panels with constant interpolation of variables. Then, evaluating the discretized BIE at every collocation point, one for an element, an overall linear equation system $Ax = b$ is set up. In the linear system, discretized $\vec{E}$ and $\partial\vec{E}/\partial n$ (one for a panel), and discretized φ (one for a vertex) are the unknowns to be solved. Fig. 2 shows a surface discretization with six panels, and the discretized unknowns are labeled.

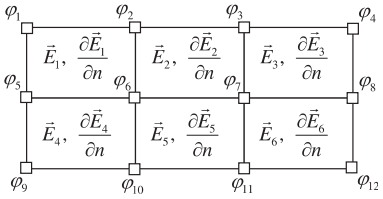

Fig. 2. The discretization and unknowns of a conductor surface.

Finally, the overall coefficient matrix A is

$$\left[\begin{array}{ccccccc} P_1 & 0 & 0 & -D_1 & 0 & 0 & 0 \\ 0 & P_1 & 0 & 0 & -D_1 & 0 & 0 \\ 0 & 0 & P_1 & 0 & 0 & -D_1 & 0 \\ \hline T_{1x}P_0 & T_{1y}P_0 & T_{1z}P_0 & -T_{1x}D_0 & -T_{1y}D_0 & -T_{1z}D_0 & A_{t1} \\ T_{2x}P_0 & T_{2y}P_0 & T_{2z}P_0 & -T_{2x}D_0 & -T_{2y}D_0 & -T_{2z}D_0 & A_{t2} \\ \hline 0 & 0 & 0 & N_{ncx} & N_{ncy} & N_{ncz} & 0 \\ N_{cx} & N_{cy} & N_{cz} & 0 & 0 & 0 & 0 \\ C_{dx} & C_{dy} & C_{dz} & C_x & C_y & C_z & 0 \\ 0 & 0 & 0 & 0 & 0 & 0 & I_c \end{array}\right] \tag{7}$$

where $N_{nc\alpha}$ $(\alpha = x, y, z)$ are matrices formed by x, y, z coordinates of the unit normal vectors at non-contact panels, and $N_{c\alpha}$ $(\alpha = x, y, z)$ are matrices formed by x, y, z coordinates of the unit normal vectors at contact panels. $T_{1\alpha}$ $(\alpha = x, y, z)$ are diagonal matrices with diagonal entries being the x, y, z coordinates of a unit tangential vector of panel, while another set of orthogonal tangential vectors of panel form the diagonal matrices $T_{2\alpha}$ $(\alpha = x, y, z)$, and A_{t1} and A_{t2} are two finite difference matrices. C_α and $C_{d\alpha}$ $(\alpha = x, y, z)$ are the matrices formed by the coefficients of $\partial E_\alpha/\partial n$ and E_α $(\alpha = x, y, z)$ in a surface form equation of current conservation. I_c is an identity matrix of $U_c \times U$, where U_c is the number of contact vertices [15].

The first three rows of (7) are from (4) in three directions $\hat{x}$, $\hat{y}$ and $\hat{z}$; the following two rows are from (6) in two tangential directions, and all non-zero items in the other rows are sparse matrices which are only dependent on geometries of conductor surfaces. So, in calculating the coefficient matrix A, most work lies in computing the dense coefficient matrices of the discretized BIEs transformed from (4) and (6). The entries in these dense matrices are in the forms:

$$\begin{cases} P_1(a,b) = \int_{panel_b} \dfrac{\mathrm{e}^{-\mathrm{i}kr(\mathbf{y}_a,\mathbf{x})}}{4\pi r(\mathbf{y}_a,\mathbf{x})}\mathrm{d}\mathbf{x}, \\ D_1(a,b) = \int_{panel_b} \dfrac{\partial}{\partial n_x}\left[\dfrac{\mathrm{e}^{-\mathrm{i}kr(\mathbf{y}_a,\mathbf{x})}}{4\pi r(\mathbf{y}_a,\mathbf{x})}\right]\mathrm{d}\mathbf{x}, \\ P_0(a,b) = \int_{panel_b} \dfrac{1}{4\pi r(\mathbf{y}_a,\mathbf{x})}\mathrm{d}\mathbf{x}, \\ D_0(a,b) = \int_{panel_b} \dfrac{\partial}{\partial n_x}\left[\dfrac{1}{4\pi r(\mathbf{y}_a,\mathbf{x})}\right]\mathrm{d}\mathbf{x}, \end{cases} \tag{8}$$

where a, b are the indexes of the panels, $panel_b$ is the integral surface of the bth panel. $\mathbf{y}_a$ stands for the collocation point in the ath panel.

3. The mixed surface integral formulation

Different from transforming the vector Helmholtz equation (1) into (4), we propose to transform (1) into indirect BIEs by introducing the imaginary dipoles. This is the basic point of our mixed surface integral formulation.

Eq. (1) is firstly rewritten as the following three independent scalar Helmholtz equations under the Cartesian coordinate system:

$$\nabla^2 E_x - \mathrm{i}\omega\mu\sigma E_x = 0, \tag{9}$$

$$\nabla^2 E_y - \mathrm{i}\omega\mu\sigma E_y = 0, \tag{10}$$

$$\nabla^2 E_z - \mathrm{i}\omega\mu\sigma E_z = 0. \tag{11}$$

Without loss of generality, taking (9) as an example, below we transform it into an indirect formulation.

Assuming that a conductor domain Ω_i^- surrounded by Γ_i is a simple connected area, an imaginary dipole distribution $\mu_x(\mathbf{x})$ on Γ_i is imposed, and the dipole axis coincides with the direction of the unit out normal at point $\mathbf{x}$, i.e. $\hat{n}(\mathbf{x})$, illustrated in Fig. 3. From potential theory [10,11], for any evaluation point $\mathbf{y}$ in Ω_i^-, the electric field in $\hat{x}$ direction $E_x(\mathbf{y})$ can be represented by the double-layer potentials produced by the imaginary dipole distributions:

$$E_x(\mathbf{y}) = \int_{\Gamma_i} \frac{\partial G_1(\mathbf{y},\mathbf{x})}{\partial n(\mathbf{x})} \mu_x(\mathbf{x})\,\mathrm{d}S_x. \tag{12}$$

Furthermore, if assuming that $E_x(\mathbf{y})$ is differentiable at point $\mathbf{y}$, one can obtain

$$\frac{\partial E_x(\mathbf{y})}{\partial n(\mathbf{y})} = \frac{\partial}{\partial n(\mathbf{y})}\left[\int_{\Gamma_i} \frac{\partial G_1(\mathbf{y},\mathbf{x})}{\partial n(\mathbf{x})} \mu_x(\mathbf{x})\,\mathrm{d}S_x\right], \tag{13}$$

where $\hat{n}(\mathbf{y})$ is any unit vector at point $\mathbf{y}$ temporarily.

When point $\mathbf{y}$ is moved onto the inner boundary Γ_i, (12) and (13) become the indirect BIEs and $\hat{n}(\mathbf{y})$ stands for the unit out normal at point $\mathbf{y}$ as shown in Fig. 3. Note that singularities in (12) and (13) exist when evaluation point $\mathbf{y}$ coincides with the integral point $\mathbf{x}$.

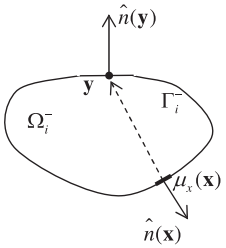

Fig. 3. The imaginary dipole on boundary induces E_x and $\partial E_x/\partial n$.

Similarly, if introducing other dipole distributions $\mu_y(\mathbf{x})$ and $\mu_z(\mathbf{x})$ on Γ_i, (10) and (11) can also be transformed into indirect integral forms, respectively:

$$E_y(\mathbf{y}) = \int_{\Gamma_i} \frac{\partial G_1(\mathbf{y},\mathbf{x})}{\partial n(\mathbf{x})} \mu_y(\mathbf{x})\,\mathrm{d}S_x,$$

$$E_z(\mathbf{y}) = \int_{\Gamma_i} \frac{\partial G_1(\mathbf{y},\mathbf{x})}{\partial n(\mathbf{x})} \mu_z(\mathbf{x})\,\mathrm{d}S_x,$$

$$\frac{\partial E_y(\mathbf{y})}{\partial n(\mathbf{y})} = \frac{\partial}{\partial n(\mathbf{y})}\left[\int_{\Gamma_i} \frac{\partial G_1(\mathbf{y},\mathbf{x})}{\partial n(\mathbf{x})} \mu_y(\mathbf{x})\,\mathrm{d}S_x\right],$$

$$\frac{\partial E_z(\mathbf{y})}{\partial n(\mathbf{y})} = \frac{\partial}{\partial n(\mathbf{y})}\left[\int_{\Gamma_i} \frac{\partial G_1(\mathbf{y},\mathbf{x})}{\partial n(\mathbf{x})} \mu_z(\mathbf{x})\,\mathrm{d}S_x\right]. \tag{14}$$

After obtaining the indirect forms of $\vec{E}$ and $\partial\vec{E}/\partial n$, namely (12), (13) and (14), substituting them into the boundary integral equations (except (4)) and boundary conditions in Table 1, we can get a set of mixed BIEs. Here, the *mixed* implies that the indirect BIEs within conductors are used to replace the unknowns of $\vec{E}$ and $\partial\vec{E}/\partial n$, while the direct BIEs among conductors are employed in the final equation system.

With the mixed formulation, the discretization and unknowns of a conductor surface are illustrated in Fig. 4, where unknown vector $\vec{\mu}$ stands for the unknowns (μ_x, μ_y, μ_z).

Finally, the left hand of the linear system becomes

$$\begin{bmatrix} T_{1x}Q_1 & T_{1y}Q_1 & T_{1z}Q_1 & A_{t1} \\ T_{2x}Q_1 & T_{2y}Q_1 & T_{2z}Q_1 & A_{t2} \\ Q_{2x} & Q_{2y} & Q_{2z} & 0 \\ N_{ncx}D_1 & N_{ncy}D_1 & N_{ncz}D_1 & 0 \\ N_{cx}D_2 & N_{cx}D_2 & N_{cx}D_2 & 0 \\ 0 & 0 & 0 & I_c \end{bmatrix} \begin{bmatrix} \mu_x \\ \mu_y \\ \mu_z \\ \varphi \end{bmatrix}, \tag{15}$$

where

$$Q_1 = P_0D_2 - D_0D_1,$$

$$Q_{2\alpha} = C_{d\alpha}D_2 + C_\alpha D_1, \quad \alpha = x, y, z,$$

$$D_2(a,b) = \frac{\partial}{\partial n(\mathbf{y}_a)} \int_{panel_b} \frac{\partial}{\partial n_x}\left[\frac{\mathrm{e}^{-\mathrm{i}kr(\mathbf{y}_a,\mathbf{x})}}{4\pi r(\mathbf{y}_a,\mathbf{x})}\right] \mathrm{d}\mathbf{x}.$$

Note that

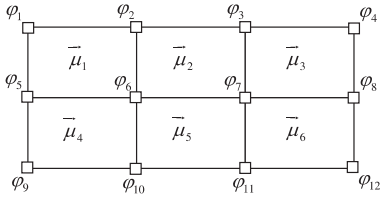

Fig. 4. The surface discretization and unknowns in the mixed method.

$$D_2(a,b) = -\hat{n}(\mathbf{y}_a)\cdot\int_{panel_b}\nabla_y\left\{\nabla_x\left[\frac{e^{-ikr(\mathbf{y}_a,\mathbf{x})}}{4\pi r(\mathbf{y}_a,\mathbf{x})}\right]\cdot\hat{n}(\mathbf{x})\right\}d\mathbf{x},$$

where ∇_y and ∇_x denote the gradient operators according to y and x, respectively. The calculation of $D_2(a,b)$ involves the hypersingular boundary integral when $a=b$. If calculating this hypersingular integral with the 2D Gauss–Legendre integral scheme, one cannot achieve sufficient accuracy even with a large number of Gauss points. Ref. [12] proposed an efficient algorithm for this kind of hypersingular integral, where the hypersingular boundary integral simply equals to the sum of a regular double integral and a regular 1D integral [12]. This algorithm is adopted here to handle the integral D_2. Now, as shown in (15) the number of unknowns has been cut down successfully to $3N+U$, from $6N+U$.

There are several important notes about this method. First, it is necessary to restrict the Ω_i^- to a simple connected area. The double-layer potential cannot get a unique solution in multiple connected domain [11]. Fortunately, for the interconnects in very large-scale integrated (VLSI) circuits, most conductor geometries satisfy this constraint. Second, the imaginary dipoles $\vec{\mu}$ have no concrete physical meaning. They are produced from the potential theory, and the indirect formulae are totally equivalent to the direct BIE for the Helmholtz equation in mathematics. Last, the only difference between the mixed method and the method in [5] lies in handling $\vec{E}$ and $\partial\vec{E}/\partial n$ in different ways, and from the second point they are equivalent in mathematics.

4. Numerical results

The proposed mixed method is implemented in C++ language. For comparing the speed fairly, we also implement the direct BIE based method. The former is denoted by MBEM and the latter by DBEM. The overall linear systems are solved by the Matlab backslash operator. In the experiments, two interconnect structures are simulated under MQS assumption. The conductor surfaces are discretized into constant rectangular panels, with collocation point located in the center of each panel. To guarantee the accuracy of nearly singular integrals, a 2D Gauss–Legendre integral scheme with 20×20 Gauss points is used for both MBEM and DBEM. The strong singular and hypersingular integrals in coefficient matrices are calculated as [12,13]. In both examples, when frequency $f\geqslant10\,\text{GHz}$ ($1\,\text{GHz}=10^9\,\text{Hz}$), the approach for computing the conductor currents is switched to sum up the magnetic fields surrounding the conductor ends [5,15].

4.1. A single wire

The dimension of this example is $1\,\mu\text{m}\times1\,\mu\text{m}\times8\,\mu\text{m}$ ($1\,\mu\text{m}=10^{-6}\,\text{m}$), and the surface is discretized with a $3\times3\times12$ mesh (162 panels) as shown in Fig. 5. The numbers

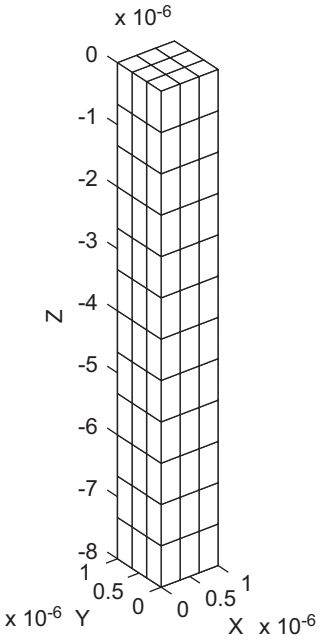

Fig. 5. A single rectangle wire.

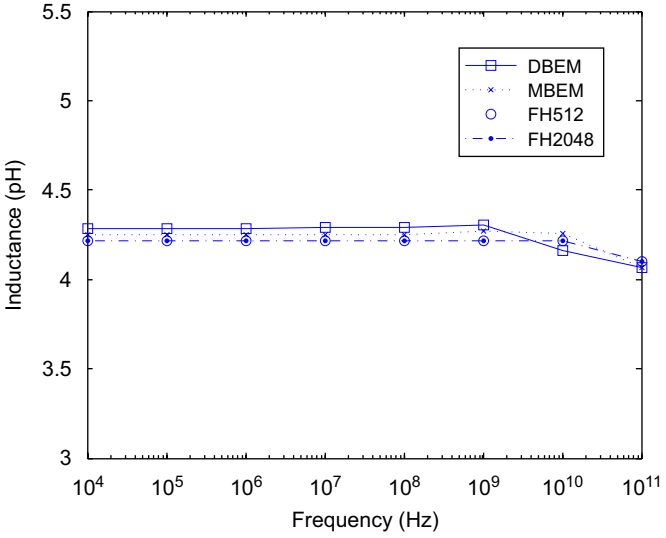

Fig. 6. Frequency-dependent inductance of the single wire.

of unknowns are 650 in MBEM and 1136 in DBEM. The impedance of the wire is calculated with the DBEM, MBEM and FastHenry [14], a famous inductance extractor based on the PEEC method, for the frequency varying from 10 KHz ($1\,\text{KHz}=10^3\,\text{Hz}$) to 100 GHz. The calculated resistance and inductance with MBEM are very close to those from other methods. The results of inductance are shown in Fig. 6, where FastHenry's results with two different discretization are shown (for example, "FH512" denotes the FastHenry's result with 512 filaments).

From Fig. 6, we can see that the inductances obtained by MBEM have little difference to those by DBEM and

FastHenry, on the whole frequency range. The maximal relative error between MBEM and FastHenry is only 1.3%, which occurs when $f = 1$ GHz.

For this structure, the skin depth at frequency $f = 100$ GHz is $\delta = 0.2\,\mu$m, which is much less than the section dimension 1 μm. And because there is only one conductor, the variation of inductance and resistance at 100 GHz just reflects the skin effect of high frequency. So, this example testifies our method on capturing the skin effect.

4.2. A 2 × 2 crossover

The dimension and discretization of this example is shown in Fig. 7, and it is the same as the "*bus*2 × 2" example in FastImp's test cases [4]. The number of panels is 256, and the numbers of unknowns are 1032 in MBEM and 1800 in DBEM. Because there are four conductors, the whole results of inductance should be a 4 × 4 matrix.

Again, the results of MBEM and DBEM coincide with each other well on the entire frequency range. We plot the mutual inductances of parallel conductors, i.e. the entry (1,2) in the inductance matrix, in Fig. 8.

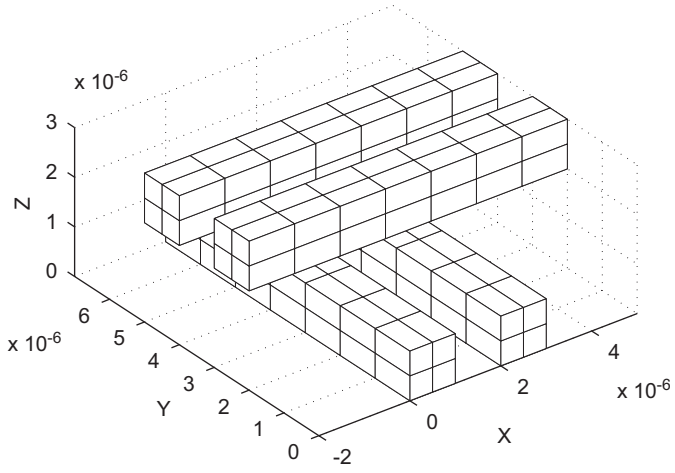

Fig. 7. A 2 × 2 crossover structure.

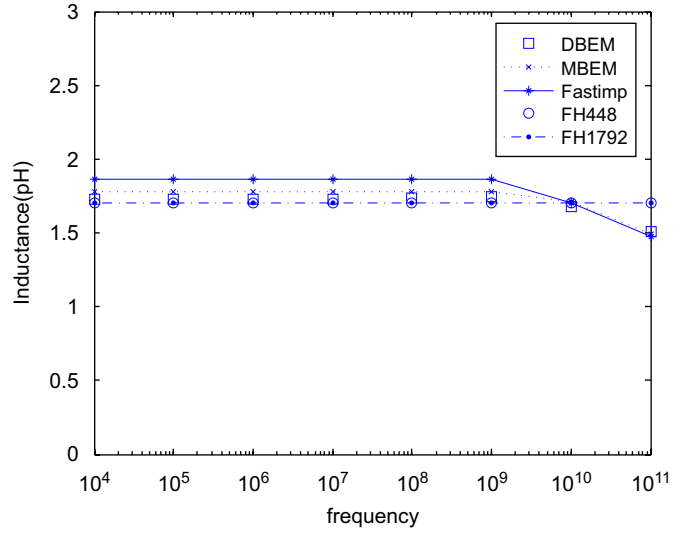

Fig. 8. Mutual inductance of parallel wires in the 2 × 2 crossover.

However, the maximal discrepancy in the results from MBEM and FastHenry with 1792 filaments is up to 15% at $f = 100$ GHz (see Fig. 8). In fact, the result of FastHenry with denser discretization (7168 filaments) does not make a difference, either. To evaluate this phenomena, we also use the FastImp from [4] to calculate this example (see Fig. 8). With FastImp's results, we find out that the results of MBEM are very accurate, whereas FastHenry should be considered to have a large error for this high-frequency situation. Besides, this experiment shows that our MBEM captures the high-frequency variation of mutual inductance very well.

4.3. Time comparison

CPU times of the two examples are listed in Table 2. For the single wire example, although on solving $Ax = b$, MBEM is faster than DBEM, the total time of MBEM is slower because it spends much more time on the integrals in D_2 than that for P_1 of DBEM. And, the time for calculating integrals occupies the majority of the total time, while solving the linear system is fast because of the small number of unknowns (650 or 1136). In both MBEM and DBEM, the accurate 2D Gauss integral scheme with 400 G points on each panel takes too much CPU time, which makes the time of calculating integrals dominate the total time.

In the example of 2 × 2 crossover, the MBEM shows its speed merit clearly. Although the numbers of unknowns in MBEM and DBEM are not very large either, namely 1032 and 1800, the difference on time consumed for solving $Ax = b$ is notable enough, i.e. 11.8 s vs 2.1 s for each right-hand side. For actual structure with multiple conductors, the advantage of fewer unknowns in MBEM will be remarkable because a large linear system has to be solved for many times. And, MBEM can be several times faster than the DBEM.

Although employing the same surface integral formulation, FastImp in [4] is much faster than the DBEM implemented by us. This is because that, in FastImp the

Table 2
The detailed breakdown of the CPU time for one frequency point(s)

	Single wire		2 × 2 crossover	
	DBEM	MBEM	DBEM	MBEM
Calculate matrix P_0, D_0	1.859	2.359	4.500	4.953
Calculate matrix D_1, P_1/D_2	12.328	22.782	7.547	12.484
Generate $Ax = b$	0.141	0.562	0.344	0.828
Solve $Ax = b$	2.828	0.546	47.063	8.515
Postprocess	0.000	0.000	0.000	0.063
Total	17.156	26.249	59.454	26.843

numerical integrals are reduced to 1D Gauss integrals with much fewer Gauss points, and a pre-corrected fast Fourier transform (pFFT) algorithm is used to accelerate integral calculation and equation solving. Therefore, it is unfair to compare the computing time of FastImp and our MBEM directly. However, the algorithms in FastImp are also applicable to MBEM, without affecting the benefit from the mixed formulation.

5. Conclusions

This paper presents a mixed surface integral formulation for calculating frequency-dependent inductance of 3D interconnects. Since the scalar Helmholtz equation can be transformed into an indirect BIE, we derive three indirect BIEs with unknowns of fictitious dipole from the vector Helmholtz equation for each conductor domain. With these indirect BIEs, the six unknowns of electric field and its normal derivative are represented by the expressions of only three dipole unknowns. Therefore, the total number of unknowns is reduced to about $4N$, from $7N$ for the surface integral formulation employing direct BIEs. Numerical experiments show that the mixed method speeds up the process of solving the linear system remarkably.

To improve the mixed method further, we will combine it with the fast algorithms in FastImp in the future.

Acknowledgments

The authors acknowledge the financial support from National Natural Science Foundation of China under Contract nos. 90407004 and 60401010. The work was also partially supported by Basic Research Foundation of TNList.

References

[1] Yu W, Wang Z, Hong X. Preconditioned multizone boundary element analysis for fast 3D electric simulation. Eng Anal Bound Elem 2004;28:1035–44.

[2] Brennan PA, Raver N, Ruehli A. Three dimensional inductance computations with partial element equivalent circuits. IBM J Res Dev 1979;23:661–8.

[3] Daniel L, Sangiovanni-Vincentelli A, White J. Using conduction modes basis functions for efficient electromagnetic analysis of on-chip and off-chip interconnect. In: Proceedings of design automation conference; 2001. p. 563–6.

[4] Zhu Z, Song B, White J. Algorithms in FastImp: a fast and wide-band impedance extraction program for complicated 3-D geometries. IEEE Trans Comput Aided Des 2005;24(7):981–98.

[5] Wang J, White J. A wide frequency range surface integral formulation for 3-D RLC extraction. In: Proceedings of international conference on computer-aided design; 1999. p. 453–7.

[6] Zhu Z, Huang J, Song B, White J. Improving the robustness of a surface integral formulation for wide-band impendance extraction of 3-D structures. In: Proceedings of international conference on computer-aided design; 2001. p. 592–7.

[7] Fang S, Wang Z. A minimum-order boundary element method to extract the 3-D inductance and resistance of the interconnects in VLSI. Sci China, Ser F 2002;45(6):453–61.

[8] Mayergoyz ID. Boundary integral equation of minimum order for the calculation of three-dimensional eddy current problems. IEEE Trans Magn 1982;18:536–9.

[9] Yuan J, Kost A. A three-component boundary element algorithm for three-dimensional eddy current calculation. IEEE Trans Magn 1994;30:3028–31.

[10] Zhu J. Boundary element analysis of elliptic boundary value problem. Beijing: Science Press; 1991 (in Chinese).

[11] Athanasiadis G. Direct and indirect boundary element methods for solving the heat conduction problem. Comput Meth Appl Mech 1985;49:37–54.

[12] Guiggiani M, Krishnasamy G, Rudolphi TJ, Rizzo FJ. A general algorithm for the numerical solution of hypersingular boundary integral equations. J Appl Mech, ASME 1992;59:604–14.

[13] Guiggiani M, Gigante A. A general algorithm for multidimensional Cauchy principal value integrals in the boundary element method. J Appl Mech, ASME 1990;57:906–15.

[14] Kamon M, Tsuk MJ, White J. Fasthenry: a multipole-accelerated 3-D inductance extraction program. IEEE Trans Microwave Theory Tech 1994;42(9):1750–8.

[15] Wang J. A new surface integral formulation of EMQS impedance extraction for 3-D structures. PhD dissertation, Massachusetts Institute of Technology, Cambridge, MA; 1999.